Princeton Plasma Physics Laboratory

PPPL- 4840

PPPL- 4840

Instability, Collapse and Oscillation of Sheaths Caused by Secondary Electron Emission

M.D. Campanell, A.V. Khrabrov and I.D. Kaganovich

January, 2013

PPPL PRINCETON PLASMA PHYSICS LABORATORY

Prepared for the U.S. Department of Energy under Contract DE-AC02-09CH11466.

Princeton Plasma Physics Laboratory
Report Disclaimers

Full Legal Disclaimer

Trademark Disclaimer

PPPL Report Availability

Princeton Plasma Physics Laboratory:

http://www.pppl.gov/techreports.cfm

Office of Scientific and Technical Information (OSTI):

http://www.osti.gov/bridge

Related Links:

U.S. Department of Energy

Office of Scientific and Technical Information

Fusion Links

Instability, Collapse and Oscillation of Sheaths Caused by Secondary Electron Emission

M. D. Campanell[a)], A. V. Khrabrov and I. D. Kaganovich
Princeton Plasma Physics Laboratory, Princeton University, Princeton, New Jersey 08543, USA

The Debye sheath is shown to be unstable under general conditions. For surface materials with sufficient secondary electron emission (SEE) yields, the surface's current-voltage characteristic has an unstable branch when the bulk plasma temperature (T_e) exceeds a critical value, or when there are fast electron populations present. The plasma-surface interaction becomes dynamic where the sheath may undergo spontaneous transitions or oscillations. Using particle-in-cell simulations, we analyze sheath instabilities occurring in a high T_e plasma slab bounded by walls with SEE. As the plasma evolves, whenever the sheath enters an unstable state, its amplitude rapidly collapses, allowing a large flux of previously trapped electrons to hit the wall. These hot electrons induce more than one secondary on average, causing a net loss of electrons from the wall. The sheath collapse quenches when the surface charge becomes positive because the attractive field inhibits further electrons from escaping. Sheath instabilities influence the current balance, energy loss, cross-B-field transport and even the bulk plasma properties. Implications for discharges including Hall thrusters are discussed. More generally, the results show that common theories that treat emission as a fixed (time-independent) "coefficient" do not capture the full extent of SEE effects.

a) Author to whom correspondence should be addressed. Electronic mail: mcampane@princeton.edu

I. INTRODUCTION

Secondary electron emission (SEE) is important in a wide variety of applications. Most theoretical treatments of plasma-surface interaction (PSI) with SEE[1,2,3,4,5,6] assume implicitly that the sheath is stable by postulating a static sheath structure with constant "emission coefficient" $\gamma_{net} \equiv \Gamma_{e,out}/\Gamma_{e,in}$, the ratio of emitted flux to incident electron flux at the surface. For floating surfaces, current balance requires

$$\Gamma_{ion} = \Gamma_{e,net} = \Gamma_{e,in} - \Gamma_{e,out} = \Gamma_{e,in}(1-\gamma_{net}). \quad (1)$$

For a given plasma source beyond the surface, $\Gamma_{e,in}$ is a (decreasing) function of the sheath potential Φ. (We define Φ as a positive quantity.) Γ_{ion} is a constant, i.e. independent of Φ, by the Bohm criterion. A larger γ_{net} requires more plasma electrons to reach the surface to balance Γ_{ion}. This leads to the well known reduction of the floating potential and increased plasma energy loss due to SEE. In analytical models or fluid simulations of specific systems, SEE is usually treated as a constant correction factor representing the enhanced heat transmission coefficient at the sheath boundary[4]. However, with SEE a stable sheath may not exist; in this case no time-independent model with a fixed γ_{net} can fully describe the PSI physics.

The question of stability should always be considered in practice. Nonsteady surface effects due to SEE have been observed in numerous plasma simulations[7,8,9,10,11,12,13,14] and experiments[15,16,17]. Because the plasma properties in any device are coupled to the PSI, this can affect more than just the surface. Instabilities attributed to SEE may cause sudden changes to the whole plasma[7,9,10], enhance cross-B-field transport[9,10,13] and drive spontaneous oscillations[8,9,15] which can modulate critical parameters (wall fluxes, energy loss, plasma potential, total plasma energy, *etc.*), launch plasma waves, produce electromagnetic radiation and cause interference.

It is therefore important to determine whether nonsteady surface effects are the norm in applications where SEE is strong. One way SEE can trigger dynamic sheaths is by making the net differential resistance of the sheath negative, causing instability of the sheath. The simplest example of this is when a high energy electron beam is incident on the surface. The emitted current induced by the beam depends on the beam impact energy, which varies with surface potential in a way that gives the current-voltage (I-V) trace an unstable branch[15]. It is natural to ask whether a similar mechanism could generate dynamic sheath behavior in any plasma-wall system with SEE, since plasma electrons can be considered a superposition of beams to an extent.

The purpose of this paper is to demonstrate the causes and consequences of SEE-induced sheath instabilities in a general theoretical framework. We will study in detail why instabilities occur, under what conditions, how they evolve in time and what effects they have on PSI. In Section II, we show that the I-V stability requirement for a static sheath can be expressed mathematically in a simple way as a competition between two terms. From this we show that the stability requirement is violated under common conditions in plasma applications. In Section III, we study the time-evolution of the sheath structure during instability in a simple simulated plasma slab. In Section IV, we discuss implications of sheath instability on PSI and some possible connection to experiments, in particular to the SEE-driven transport observed in Hall thrusters.

II. MECHANISM OF SHEATH INSTABILITY

A. General Considerations

Although the term "sheath" refers to the region of positive space charge in front of the surface or "wall", the essential force that draws ions to the wall and repels incoming plasma electrons is provided by the negative charge on the wall. Let σ_e denote the negative surface charge density. (This way for convenience we have σ_e and Φ as positive quantities for a classical sheath with negatively charged wall and negative surface potential.)

The sheath is I-V stable[18] at an equilibrium surface potential relative to the plasma Φ_{eq} if $d\Gamma_{e,net}/d\Phi < 0$ at $\Phi = \Phi_{eq}$, (or equivalently if $d\Gamma_{e,net}/d\sigma_e < 0$ at $\sigma_e = \sigma_{e,eq}$). The reason is that any perturbation of Φ will perturb $\Gamma_{e,net}$ in a way that serves to restore Φ to Φ_{eq}. On the other hand, the sheath cannot be a static structure if $d\Gamma_{e,net}/d\Phi > 0$ because perturbations of the surface charge would amplify. For a floating surface, Φ_{eq} is the value of Φ satisfying the zero current condition (1). For a conducting surface, nonzero currents are allowed in some configurations. For instance, if a plasma-facing surface is inductively coupled to a conductor biased at (negative) potential -V, then $\Phi_{eq} = V$. Hence any value of Φ_{eq} is possible depending on the system. The stability condition is a *separate* requirement.

To determine whether the sheath is stable for some Φ requires computing $\Gamma_{e,net}$ as a function of Φ. For a given interior electron energy distribution function (EEDF) over kinetic energies parallel and normal to the wall $f(w_{//},w_\perp)$, along with $\gamma(\varepsilon)$, the SEE yield as a function of kinetic impact energy ε, $\Gamma_{e,net}$ can be written as,

$$\Gamma_{e,net} = \int_0^\infty \int_{e\Phi}^\infty f(w_{||}, w_\perp)[1-\gamma(w_{||}+w_\perp - e\Phi)]dw_\perp dw_{||}. \quad (2)$$

The form of (2) indicates that electrons in the plasma interior with $w_\perp \geq e\Phi$ will reach the wall and have impact energy $\varepsilon = w_{//} + w_\perp - e\Phi$. Differentiating with respect to Φ yields two terms,

$$\frac{d\Gamma_{e,net}}{d\Phi} = -\int_0^\infty f(w_{||}, e\Phi)[1-\gamma(w_{||})]dw_{||} + e\int_0^\infty \int_{e\Phi}^\infty f(w_{||}, w_\perp)\frac{d\gamma}{d\varepsilon}(w_{||}+w_\perp - e\Phi)dw_\perp dw_{||} \quad (3)$$

The stability condition can be expressed in a lucid form. First, let us write the electron flux as a summation to treat cases where there may be multiple electron components in the source distribution (e.g. a plasma with a beam). Let $\Gamma_{S,in}(\Phi)$ denote the total influx of component "S". The differential electron flux terms in (3) can be rewritten in terms of the influx to express the stability condition as,

$$\frac{d\Gamma_{e,net}}{d\Phi} = \sum_S \left[\frac{d\Gamma_{S,in}}{d\Phi}\left(1-\gamma_{//,S}\right) + \Gamma_{S,in}\left\langle \frac{d\gamma}{d\varepsilon}\right\rangle_S \right] < 0. \quad (4)$$

Equation (4) gives general insight into the physics of stability. The first "collection" term is due to the change in number of electrons that reach the surface as Φ varies, $d\Gamma_{S,in}/d\Phi$. Because marginally collected electrons with $w_\perp \approx e\Phi$ in the plasma interior will strike the wall with zero normal kinetic energy, their average SEE yield $\gamma_{//,S}(\Phi)$ is due only to their $w_{//}$, as seen in the first integral of (3). Because it is always true that $d\Gamma_{S,in}/d\Phi \leq 0$, the collection term is stabilizing (provided $\gamma_{//,S} < 1$). This is why sheaths without SEE are I-V stable and can exist statically.

The second "energy" term of (4) is the change in emission caused by the change in impact energy of the incident electrons as Φ varies. Quantitatively as seen in the second integral of (3), the energy term is just the influx $\Gamma_{S,in}$ times the average of $d\gamma(\varepsilon)/d\varepsilon$ over the influx. The energy term is usually destabilizing because $d\gamma(\varepsilon)/d\varepsilon > 0$ for materials in the energy range of interest. Thus overall, the collection term must outweigh the energy term for a static sheath to exist with $d\Gamma_{e,net}/d\Phi < 0$.

B. Instability Due to Fast Electrons or Beams

An elegant example of the competition between terms in (4) is Griskey and Stenzel's experiment[15]. A ~200eV electron beam was projected towards an electrode immersed in a cold T_e ~ 3eV background plasma. The I-V trace of this electrode had a negative (unstable) differential resistance in the voltage range where all beam electrons were collected and no plasma electrons were collected. For instance at -100V, the collection term of (4) is clearly zero for both the beam and plasma electron components, so the beam's energy term drives instability. It was shown that spontaneous oscillations would arise if the electrode were inductively coupled to a grid biased to a potential in the unstable branch of the I-V trace. On the other hand, the differential resistance was positive for electrode voltages where plasma or beam electrons were *partially* collected (e.g. near -200V or near -1V) because the respective collection term in (4) outweighed the energy term(s).

There were three floating potentials satisfying zero current. Two were in the voltage branches where beam and plasma electrons were partially collected, both stable. The third was near -100V in the unstable I-V branch, meaning it would not be observable on an unbiased floating surface. The concepts in this example are important in various systems where fast electrons are present among the colder plasma electrons. For instance, a qualitatively similar I-V trace can be measured for probes in plasmas ionized by energetic electrons emitted from hot biased filaments[19].

C. Instability in Hot Plasmas

For higher temperature plasma applications, the SEE induced by thermal plasma electrons becomes important. To examine stability in such systems, we first consider a simple example; a 1-D Maxwellian source EEDF in front of a wall (with no parallel energy $w_{//}$).

$$f(w_\perp) = n_0 \left(\frac{m_e}{2\pi T_e} \right)^{1/2} \exp(-w_\perp / T_e) \tag{5}$$

To illustrate the basic physics, we use an approximate function for the SEE yield. If we let $\gamma(\varepsilon) = \varepsilon/\varepsilon_1$, where ε_1 is the energy at which $\gamma(\varepsilon)$ crosses unity, $\Gamma_{max,net}(\Phi)$ can be calculated analytically,

$$\Gamma_{\max,\text{net}} = n_0 \left(\frac{m_e}{2\pi T_e} \right)^{1/2} T_e \left(1 - \frac{T_e}{\varepsilon_1} \right) \exp(-e\Phi / T_e) \tag{6}$$

Rewriting $\Gamma_{max,net}$ in terms of the influx $\Gamma_{max,in}$, the positive part of (6), gives

$$\Gamma_{\max,net} = \Gamma_{\max,in} \left(1 - \frac{T_e}{\varepsilon_1} \right) \tag{7}$$

By analogy to the general stability equation (4), the differential flux can be expressed in terms of $\Gamma_{max,in}$,

$$\frac{d\Gamma_{\max,net}}{d\Phi} = -\frac{e\Gamma_{\max,in}}{T_e} + \frac{e\Gamma_{\max,in}}{\varepsilon_1} \tag{8}$$

If $T_e < \varepsilon_1$, then $d\Gamma_{Max,net}/d\Phi < 0$ for all Φ, meaning the plasma electrons produce a positive differential resistance. Hence sheaths are unsurprisingly I-V stable in systems with low temperature plasmas. But as T_e increases, the EEDF over $w_\perp$ spreads out, thereby weakening the collection term. Beyond a critical temperature ($T_e > \varepsilon_1$), we see that $d\Gamma_{Max,net}/d\Phi > 0$ in (8). This raises the question of whether a static sheath can exist in high temperature plasmas.

It is necessary to note from (7) that when $T_e > \varepsilon_1$, the emission coefficient of the Maxwellian electrons $\gamma_{Max} = T_e/\varepsilon_1$ exceeds unity for all Φ. So for a floating surface, a classical Debye sheath with $\sigma_e > 0$ could not exist due to the zero current condition. Zero current can instead be maintained with a nonmonotonic potential profile $\varphi(x)$ called a "space-charge limited" (SCL) sheath[1,2,3,4,5,6,20], or by an inverse sheath[21] with a $\varphi(x)$ that monotonically *increases towards the wall*; these structures have a positive surface charge ($\sigma_e < 0$) that pulls some secondaries back to the wall. A new flux component Γ_{ref} appears in addition to the Maxwellian plasma electrons Γ_{max}, so that $\gamma_{net} < 1$ overall in (1). Analyzing stability when $\sigma_e < 0$ is more complex because surface charge perturbations will also affect Γ_{ref} and the stability equation (4) must include this species.

However, there is always a branch of surface potentials in which $\sigma_e > 0$. The I-V trace is unstable in this branch when $T_e > \varepsilon_1$. This is important for conducting surface applications where zero current is not required. For hot plasmas contacting conductors in various circuit arrangements, the same types of spontaneous oscillations demonstrated in Ref. 15 with a beam are possible and the implications discussed in that paper carry over directly.

In reality, SEE yields[22] are nonlinear, nonmonotonic functions of energy and have an angular dependence. But this does not change the conclusion. For arbitrary $\gamma(\varepsilon_{//},\varepsilon_\perp)$, the flux of a source EEDF $f(w_{//},w_\perp) = f_{//}(w_{//})f_\perp(w_\perp)$ with arbitrary $f_{//}(w_{//})$ that is Maxwellian over $w_\perp$ is,

$$\Gamma_{e,net} \propto \int_0^\infty \int_0^\infty f_{||}(w_{||}) e^{-(w_\perp^* + e\Phi)/T_\perp} [1 - \gamma(w_{||}, w_\perp^*)] dw_\perp^* dw_{||} \tag{9}$$

We started with (2), inserted $f_\perp(w_\perp)$ from (5), and then performed the change of variable $w^*_\perp = w_\perp - e\Phi$. Differentiating (9) we obtain,

$$\frac{d\Gamma_{e,net}}{d\Phi} = -\frac{e}{T_\perp} \Gamma_{e,net} \tag{10}$$

Thus if $\Gamma_{e,net} < 0$, or equivalently if the SEE coefficient exceeds unity, it follows that $d\Gamma_{e,net}/d\Phi > 0$. This is critical because it is well known that SEE coefficients for commonly used plasma-facing components can exceed unity at typical plasma temperatures[23] (in the tens of eV range and above). Eq. (10) proves that anytime this is the case, the surface has an I-V characteristic with a negative differential resistance in the voltage range where the surface is negatively charged. Sheath instability phenomena could occur in all such applications.

D. Influence of Parallel Energies on Instability

Equation (10) holds independently of the structure of the parallel component of the EEDF, $f_{//}(w_{//})$, as long as the full EEDF is separable, i.e. $f(w_{//},w_\perp) = f_{//}(w_{//})f_\perp(w_\perp)$. Parallel energies are often ignored in sheath theories because they are not altered by the sheath and do not affect $\Gamma_{e,in}$. But parallel energies enhance the SEE yield and weaken the collection term relative to the energy term via the $\gamma_{//,S}$ parameter in (4). This is relevant to all real plasmas, which have three velocity dimensions. For the case of a 3D isotropic Maxwellian, the critical T_e required for instability is much less than in the 1-D Maxwellian example from (8).

Parallel energies can also drastically alter the I-V trace for surfaces in plasmas with beams. For example, a "simple beam" with (by definition) a small spread in energy, normally incident on a surface in a plasma, will contribute a positive electron flux and positive differential resistance in part of the branch of surface voltages where the beam is partially collected. Also, provided the beam flux *approaching* the wall exceeds Γ_{ion}, the surface has a floating potential in this branch. But if the beam is incident at an oblique angle such that $\gamma_{//,beam} > 1$ in (4), it follows that the collection term is *destabilizing*. In addition, $\Gamma_{beam,net} \leq 0$ for all Φ and no floating potential can exist for the beam!

The energy term can also change its usual sign with an oblique beam. Materials that obey the universal SEE yield curve shape[22] exhibit a local maximum of $\gamma(\varepsilon)$ typically somewhere between 0.2-1 keV. Thus for most materials there is an energy range in which $d\gamma(\varepsilon)/d\varepsilon < 0$ *and* $\gamma(\varepsilon) > 1$. For beams with an energy component parallel to the wall in this range, the energy term is *stabilizing*.

E. Instability in Hot Weakly Collisional Plasmas

A high collisionality is necessary to maintain a Maxwellian EEDF. In applications where collisionality is low, some new kinetic SEE effects arise, including the possibility of secondaries propagating to other surfaces[24,29,48]. The source EEDF $f(w_{//},w_{\perp})$ in front of each surface is much different from the Maxwellian case of Sec. II.C. It turns out sheath instability still occurs at high temperature, but the mechanism is more intricate.

Consider a symmetric weakly collisional planar plasma bounded by floating walls with SEE. Such a plasma can be produced in the E×B discharge model in Fig. 1(a) at low neutral pressure. Sheaths must form at each wall in order to maintain $\Gamma_{e,net} = \Gamma_{ion}$. A potential well $\varphi(x)$ of some amplitude Φ forms, as in Fig. 1(b). Electrons with *total* energy normal to the walls $w_x \equiv \frac{1}{2}m_e v_x^2 - e\varphi(x) < e\Phi$ are trapped and oscillate in the potential well while those with $w_x > e\Phi$ can quickly escape to the walls. The electron velocity distribution function (EVDF) over $v_{//}$ and v_x in the plasma interior (where the potential energy is near zero) is shown in Fig. 1(c).

The EVDF structure forms self-consistently with the sheaths. In Fig. 1(c), the electron density is much lower beyond the cutoff velocity $|v_x| > v_{cutoff} \equiv (2e\Phi/m_e)^{1/2}$ because loss cone replenishment is weak in low collisionality. However, note there is a small high density cluster of electrons just beyond the cutoffs; this cluster consists mostly of secondaries. Secondaries are emitted from the wall, the "top" of the potential well, so they always have $w_x > e\Phi$. They are accelerated away from the wall by the sheath, have $|v_x| > v_{cutoff}$ in the interior, cross the plasma, overcome the other sheath and strike the other wall as a "beam" after a flight time τ_{flight}. Collisions will not significantly attenuate the beam if the average collision time is less than τ_{flight}.[24,29]

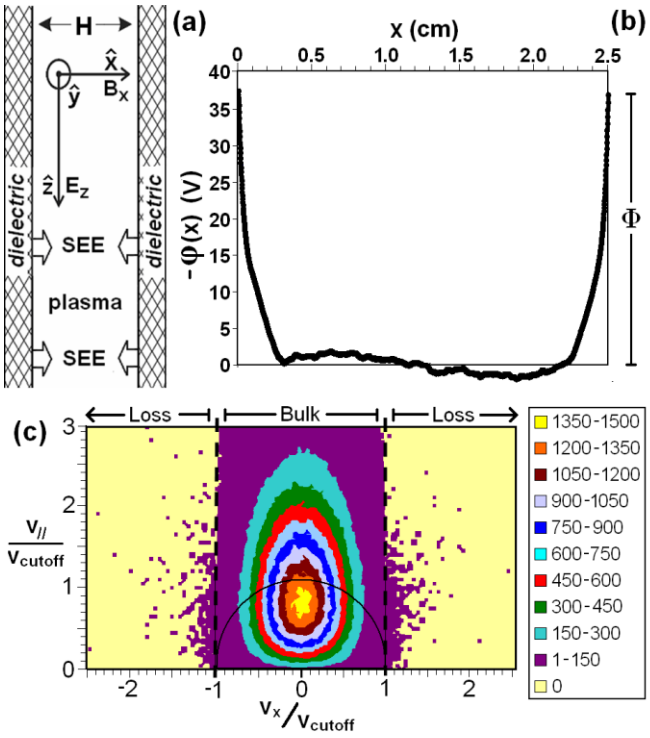

FIG. 1. (color online) (a) Simulation model discussed further in Sec. III.A. (b) Confining potential well seen by electrons, $-\varphi(x)$. Here, the plasma size H is 2.5 cm. We refer to the center (x = 1.25 cm) as the zero potential in the discussion. (c) Distribution over $v_{//}$ and v_x for electrons in the "middle" of the plasma gap (0.8cm < x < 1.7cm) in relative units. Note, $v_{//} \equiv (v_y^2 + v_z^2)^{1/2}$. In this figure Φ = 38V and $v_{cutoff} = 3.7\times10^8$ cm/s.

To treat the weakly collisional case with the generalized stability equation (4), we must consider positive and negative perturbations of Φ separately because of the EEDF discontinuity at $w_x = e\Phi$. For negative perturbations, the fact that the electron density in the bulk is orders of magnitude larger than in the loss region causes the $d\Gamma_{in}/d\Phi$ factor in (4) to be much larger than the energy term. Therefore, the sheath is unstable when the collection term itself is destabilizing, i.e. $(1 - \gamma_{//}) < 0$. This occurs when the effective electron temperature component parallel to the wall $T_{//}$ is large enough that the SEE yield of the marginally trapped "weakly confined electrons" (WCE's) γ_{WC} exceeds unity. Formally, γ_{WC} is just $\gamma_{//}$ in (4) when the derivative $d\Gamma_{e,net}/d\Phi$ is taken as $w_x \rightarrow e\Phi$ from below. Instability does not occur for positive perturbations of Φ because marginally *lost* electrons are mostly *cold* beam electrons. Positive perturbations of Φ are self-canceled by a decreased collection of beam electrons from the other wall with $\gamma_{//,beam} < 1$.

The "WCE instability" concept was verified in Ref. 9. In a simulated weakly collisional plasma, when the sheaths were stable ($\gamma_{WC} < 1$), the data showed that the plasma evolved slowly in a "quasistatic" manner over many μs. But anytime γ_{WC} reached unity, a sudden drop of Φ would occur over a few ns. The fact that Φ always drops and never *jumps*

reflects the asymmetry between positive and negative perturbations discussed above. Another special feature of the WCE instability is that electron energy parallel to the wall $w_{//}$ is essential to drive it. On the other hand, it was shown that normal energy $w_{\perp}$ alone was capable of driving instability in the Maxwellian plasma or applied beam cases.

F. What happens when a sheath is unstable?

To further understand the effects of sheath instabilities on PSI, one must study not just why they occur, but also how they evolve. A system with unstable sheaths could either undergo a transition to a stable state or oscillate perpetually. The exact behavior will depend on specifics of the plasma device including the EEDF and type of surface.

As an illustrative example, we will analyze the time evolution of a WCE sheath instability in the next section. Ref. 9 presented simulation data showing that the WCE instability caused sudden changes in plasma parameters. But the instabilities themselves, including how the sheath structure and currents evolved in time, were not examined in detail. Here, we will find that some interesting and important effects arise during instability which violate commonly accepted PSI principles.

III. ANATOMY OF A SHEATH INSTABILITY

A. Overview of the simulation code

The 1D3V electrostatic direct implicit particle-in-cell code (EDIPIC)[25] was written by D. Sydorenko to model a planar E×B xenon plasma bounded by walls with SEE, see Fig. 1(a). The code is well suited to study SEE effects because of the simple geometry and because the diagnostics track secondaries separately. The system is assumed uniform in the y-z plane. The plasma temperature is maintained by an E×B background field, which imparts energy to electrons by drift motion. This configuration resembles the acceleration region of a Hall thruster (HT)[26]. Development of EDIPIC was motivated in part by the strong experimental support of the influence of SEE in HT's which was reviewed recently by Y. Raitses *et. al*[27]. The applicability of the model for HT's is justified elsewhere [28,29,25].

The main control parameters are the uniform applied fields E_z and B_x, neutral gas density n_a, plasma density n_0, plasma width H and turbulent collision frequency ν_{turb}. Poisson's equation is solved using the direct implicit algorithm[30] to compute the plasma's self-generated presheath-sheath field $E_x(x)$. Particle dynamics are governed by $E_x(x)$ and the E×B drift from the background fields. Electrons suffer collisions with neutrals which scatter all velocity components. Turbulent collisions randomly scatter the y-z component of the velocity vector, leading to an *average* y-z directed energy gain from the axial electric field of $m_e V_D^2$ per scatter, where $V_D = E_z/B_x$ is the drift velocity. Turbulent collisions can be used to model anomalous Bohm-like transport (along **E**, across **B**) in real discharges[31]. They can also be used as an adjustable heat source for the bulk plasma. Turbulent collisions do not alter $\Gamma_{e,in}$ directly because the velocity component normal to the wall v_x is unchanged. Ionization of neutrals occurs at a rate roughly equal to the losses, so there is not much change in plasma density during the simulation. SEE in EDIPIC is implemented using properties of boron-nitride ceramics (BNC), a typical HT wall material. For BNC, $\gamma(\varepsilon) \approx 0.17\varepsilon^{1/2}$ (ε in eV) and crosses unity near ε = 35eV.[32] EDIPIC was rigorously verified to reproduce experimental plasma behaviors[25].

B. Plasma EVDF properties in a typical simulation

In Fig. 1(c), we illustrated the structure of a representative weakly collisional plasma produced in a simulation with E_z = 200 V/cm, B_x = 0.01T, $n_a = 10^{12}$ cm^{-3}, $n_0 = 1.1\times10^{11}$ cm^{-3}, $\nu_{turb} = 5.6\times10^6$ s^{-1} and H = 2.5cm. These parameters are in the range used to model HT's under experimental conditions (cf. Table I of Ref. 29).

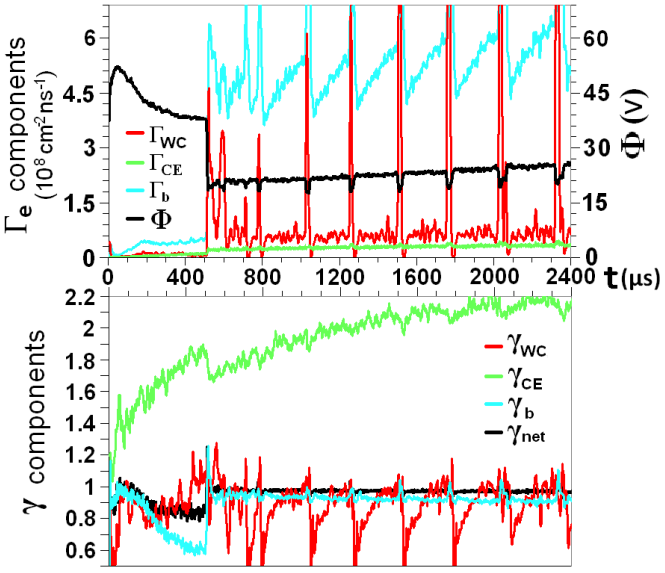

FIG. 2. (color online) Evolution of key parameters at the right wall over the first 2.4μs of the E_z = 200 V/cm simulation. Φ is the potential difference between the right wall and plasma center. The -φ(x) and EVDF plots in Fig. 1(b,c) were taken at t = 497.5ns.

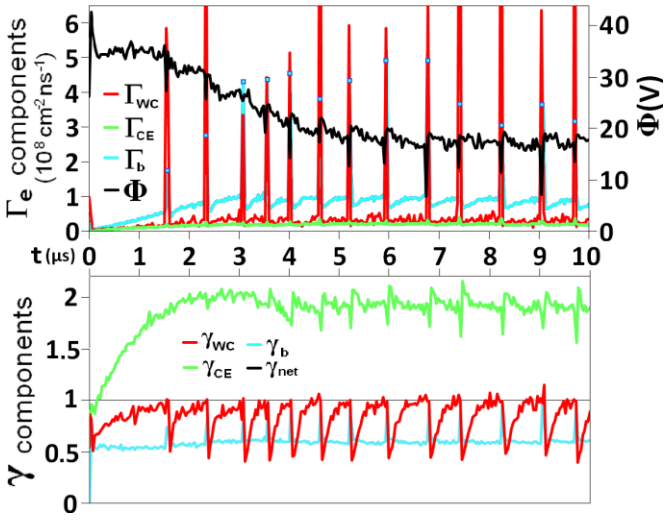

FIG. 3. (color online) A simulation with E_z = 50 V/cm, $\nu_{turb} = 5\times10^7$ s^{-1} and all other conditions the same as the E_z = 200 V/cm run. Data in this plot are averaged over 30ns intervals to smooth the fluctuations and show more clearly that $\gamma_{WC} = 1$ is the critical point of instability. Squares are used to mark the peaks of Γ_b during instability, which are hidden by the peaks of Γ_{WC}

The electron influx $\Gamma_{e,in}$ to the walls consists of several components of different origins. Trapped "bulk" electrons outside of the semicircular region in Fig. 1(c) have total velocities |v| exceeding v_{cutoff}. They can be scattered into the loss region by elastic collisions with neutrals, forming the "collision-ejected electron" (CEE) flux Γ_{CE}. The density of CEE's in the loss region is very low because the frequency of collisions ν_{en} is small. This is a common property of low pressure discharges where the mean free path is larger than the system width H. (Coulomb collisions are known to only weakly affect the plasma[25], so their contribution to scattering is less important.)

Γ_b is the SEE "beam" flux (from the opposite wall). In equilibrium by symmetry of the two beams, the "secondary" (emitted) outflux from a wall $\Gamma_{e,out}$ is also Γ_b. Therefore, $\Gamma_{e,net} = \Gamma_{e,in} - \Gamma_{e,out} = (\Gamma_{CE} + \Gamma_b) - \Gamma_b = \Gamma_{CE}$. The ion flux Γ_{ion} is estimated by the Bohm criterion in terms of T_x. Analytical estimates for $T_{//}$, T_x, Φ and flux components in *steady state* in terms of simulation parameters are given in Ref. 29. The exact values are unimportant to us here. We care about relative magnitudes for current balance. Because the walls are floating, the zero current condition applies.

$$\Gamma_{CE} \approx \Gamma_{ion} \tag{11}$$

The sheath potential Φ limits Γ_{CE} to maintain this balance. There is a second quasisteady state condition for maintenance of the beam. The SEE induced by the influx, $\gamma_{CE}\Gamma_{CE} + \gamma_b\Gamma_b$, must produce the beam reaching the other wall Γ_b, where γ_{CE} and γ_b are the average number of secondaries produced per impacting CEE and beam electron, respectively. This gives,

$$\Gamma_b \approx \frac{\gamma_{CE}\Gamma_{CE}}{1-\gamma_b} \approx \frac{\gamma_{CE}\Gamma_{ion}}{1-\gamma_b} \tag{12}$$

Secondaries are colder than bulk electrons, so $\gamma_b < \gamma_{CE}$ always. The net SEE yield γ_{net} can be derived from (12),

$$\gamma_{net} \approx \frac{\gamma_{CE}}{1+\gamma_{CE}-\gamma_b} \tag{13}$$

There is an additional way that electrons can reach the wall. Weakly confined electrons with w_x slightly below eΦ can be nudged by field fluctuations into the loss region. In EDIPIC diagnostics, impacting electrons are assumed to be WCE's if they did not come directly to the wall after a neutral collision (CEE) or after emission from the other wall (beam). In quasisteady state, the influence of Γ_{WC} on the flux balance is small because $\Gamma_{WC} << \Gamma_b$[9,29]. One can correct (11) and (12) to account for WCE's but this will not be needed here. What matters is the parameter γ_{WC} in the simulation data provides a metric for sheath stability.

Γ_b in (12) depends critically on γ_b. True secondaries are emitted with small initial kinetic energies. In transit across the plasma, they undergo drift motion in the y-z plane with $w_{//}$ oscillating between 0 and $2m_eV_D^2$. Their motion across the plasma (x-direction) is governed by φ(x). By the symmetry of φ(x), v_x upon impact at the opposite will be negligible so the beam impact energy ε_{beam} depends only on the phase of parallel drift motion at the flight time τ_{flight}[7],

$$\varepsilon_{beam} \approx m_eV_D^2(1-\cos(\omega_c\tau_{flight})), \tag{14}$$

where ω_c = eB/m is the gyrofrequency. τ_{flight} is simply a (decreasing) function of Φ. Eq. (14) does not quantify the beam energy precisely because a substantial fraction of the SEE ~0.2-0.4 consists of elastically backscattered electrons[32] with various emission energies and mixed drift phases. But the main point of (14) is γ_b can vary substantially with Φ. This coupling is critical in the simulations.

C. Long time scale plasma behavior

Fig. 2 and Fig. 3 show the temporal evolution of the flux components, their partial SEE coefficients and Φ in two simulations. The initial simulation state (t=0) is a spatially uniform Maxwellian EVDF with initial temperature 10eV in a cold ion background. Sheaths quickly form as electrons escape to the walls, the surface charges negatively and ions are then pulled to the walls. The loss cone becomes depleted within ~100ns. Eq. (13) shows that in quasisteady state, the SEE beams with $\gamma_b < 1$ create a feedback mechanism that keeps γ_{net} below 1 automatically, so that a classical sheath with a monotonic φ(x) and $\sigma_e > 0$ always forms.

Most of the plasma evolution is "quasistatic" and Eqs. (11),(12),(13) hold approximately. But there are times when the parameters in Fig. 2 and Fig. 3 abruptly change. These transitions are sheath instabilities, triggered when $\gamma_{WC} \approx 1$, as discussed previously. A negative perturbation -ΔΦ of Φ in Fig. 1(b) moves the cutoff velocity in Fig. 1(c) inwards. Now, at each wall, WCE's with $e(\Phi-\Delta\Phi) < w_x < e\Phi$ will be

able to overcome the sheath and reach the wall. When $\gamma_{WC} > 1$, the initial perturbation will lead to a net reduction of σ_e on the wall, further lowering Φ, allowing more previously trapped electrons to reach the wall *etc*. Thus we expect the sheath instability to feature a fast loss of surface electrons accompanied by a fast decrease of Φ and a fast increase of Γ_{WC}.

D. Detailed Temporal Analysis of a WCE Instability

1. Parameters used to describe instability

To investigate the sheath "collapse" closely, in Fig. 4 we zoom into the instability near t = 500ns in Fig. 2. During instabilities, the system is no longer symmetric because the two sheaths do not collapse simultaneously. We therefore follow parameters at both walls in Fig. 4 and use subscripts L and R to distinguish them in writing. We introduce the electron charging rate of each floating wall,

$$d\sigma_e/dt = e(\Gamma_{e,net} - \Gamma_{ion})$$

in Fig. 4 because the surface charges $\sigma_{e,R}$ and $\sigma_{e,L}$ determine the potential barriers Φ_R and Φ_L relative to the plasma interior. Right before sheath collapse, all parameters are at some "equilibrium value". For instance, we denote Φ_{eq} as the potential right before sheath collapse, when $\Phi_R = \Phi_L = \Phi_{eq}$.

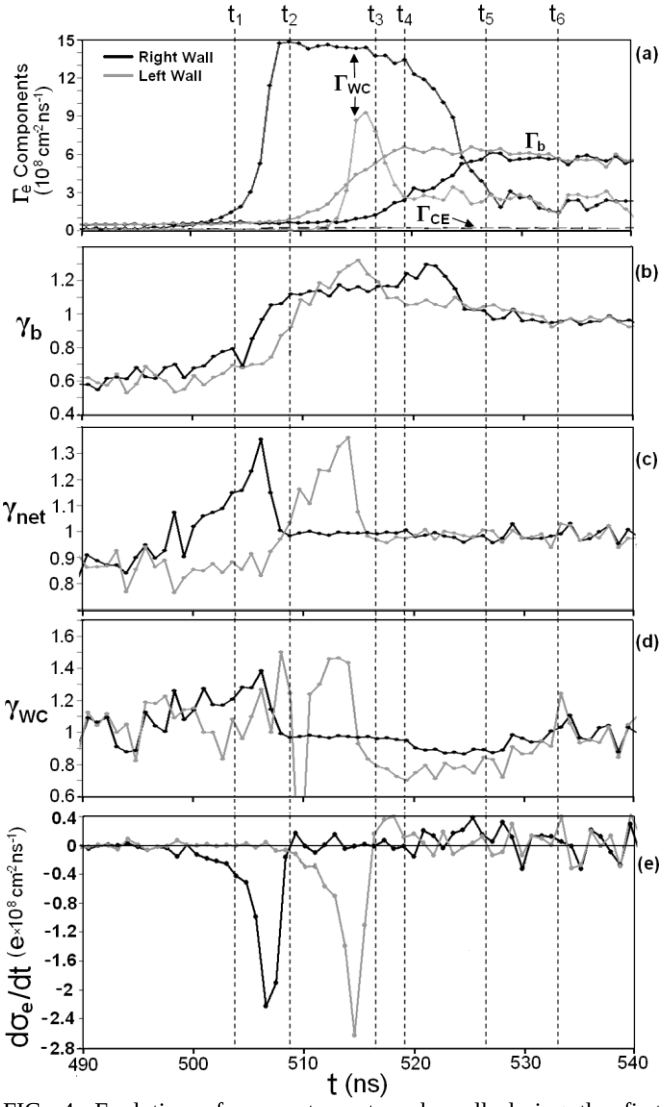

FIG. 4. Evolution of parameters at each wall during the first instability in the E_z = 200V/cm run. Temporal data are recorded every 0.88ns. (The time step for movement of particles is 1000 times smaller, 0.88ps, chosen to satisfy the Courant condition for the simulation parameters.)

2. Onset of instability – The sheaths collapse

We now analyze the instability in Fig. 4. Because γ_{WC} crossed unity near t = 490 ns, the sheaths have become unstable. Sheath collapse begins at the right wall first around t = 498ns. By t_1 = 503ns, substantial decharging of the right wall has taken place and $\Gamma_{WC,R}$ has become the dominant influx component. $\Gamma_{WC,R}$ continues to increase for as long as $d\sigma_{e,R}/dt$ is negative. This is because as σ_R (and hence Φ_R) drop, the energy range of the previously trapped electrons that can reach the wall widens, $e\Phi_R < w_x < e\Phi_{eq}$.

Let us quantify the time evolution of the sheath collapse. Before instability, the system is in a quasisteady state, so $d\sigma_{e,R}/dt \approx 0$ and $\Gamma_{WC,R}$ is at some small value $\Gamma_{WC,eq}$. The

sheath collapse at the right wall leads to a large influx of WCE's but does not affect $\Gamma_{ion,R}$, does not immediately perturb the SEE flux coming from the *left* wall from its initial value $\Gamma_{b,eq}$, and only causes $\Gamma_{CE,R}$ to increase slightly via loss cone expansion. Thus, the net charge rate is,

$$\frac{1}{e}d\sigma_e/dt \approx \Delta\Gamma_{WC}(1-\gamma_{WC}) \quad (15)$$

where we wrote $\Delta\Gamma_{WC} \equiv \Gamma_{WC} - \Gamma_{WC,eq}$. As first order linear approximations, the reduction of the potential barrier Φ should be proportional to the charge loss, $\Delta\Phi \equiv \Phi - \Phi_{eq} \approx \alpha(\sigma_e - \sigma_{e,eq}) \equiv \alpha\Delta\sigma_e$. Also, during collapse, $\Delta\Gamma_{WC} \approx -\beta\Delta\Phi$ where β depends on the density of WCE's bordering loss cone in energy space.

Now we can express $\Delta\sigma_e$ as $(-\Delta\Gamma_{WC})/\alpha\beta$ and solve the differential equation (15) for $\Delta\Gamma_{WC}(t)$ to get,

$$\Delta\Gamma_{WC}(t) = \Delta\Gamma_{WC,0}\exp[e\alpha\beta(\gamma_{WC}-1)t] \quad (16)$$

Then $\Delta\sigma_e(t)$ and $\Delta\Phi(t)$ in terms of $\Delta\Gamma_{WC}(t)$ are,

$$\Delta\Phi(t) = -e\alpha\Delta\Gamma_{WC}(t)(\gamma_{WC}-1) \quad (17)$$

$$\Delta\sigma_e(t) = -e\Delta\Gamma_{WC}(t)(\gamma_{WC}-1) \quad (18)$$

In (16), $\Delta\Gamma_{WC,0}$ is just the initial value of $\Delta\Gamma_{WC}$ due to some perturbation. When $\gamma_{WC} < 1$, perturbations are damped. But when $\gamma_{WC} > 1$, we see that Γ_{WC}, along with σ_e and Φ, should all displace exponentially in time from their equilibrium values. This appears in to be in good qualitative agreement with the right wall collapse data, Fig. 4. The process is even faster than a pure exponential for two reasons. Firstly, the coefficient β increases as Φ drops further because the density of electrons in energy space increases deeper into the bulk (Fig. 1(c)). Secondly, γ_{WC} continues increasing during collapse because WCE's hit the wall with larger v_x as Φ drops.

While the linear approximation is not exact, the analysis shows the sheath collapse is a rapid runaway effect. Another hidden approximation was that $\Gamma_{e,net}(t)$ can be expressed in terms of the bulk EEDF and $\Phi(t)$ as the sheath evolves. That is valid for dynamic sheaths provided the sheath changes slowly over the propagation time of electrons through the sheath, which is comparable to the plasma period (~0.1ns here). Hence this is acceptable for the sheath collapse. But the collapse is far too fast to be considered quasistatic because it occurs faster than the flight time of secondaries *between the walls* τ_{flight}, so the formulas describing the steady state physics (11),(12),(13), which assume $\Gamma_b = \Gamma_{e,out}$ at each wall do not apply. For instance in Fig. 4(c), $\gamma_{net,R}$ reaches well above unity to 1.33 during the collapse, in violation of (13). It would be physically impossible to have $\gamma_{net} > 1$ for a floating surface in any steady state sheath theory.

The left wall sheath collapses near t = 512ns, similarly to the right wall sheath.

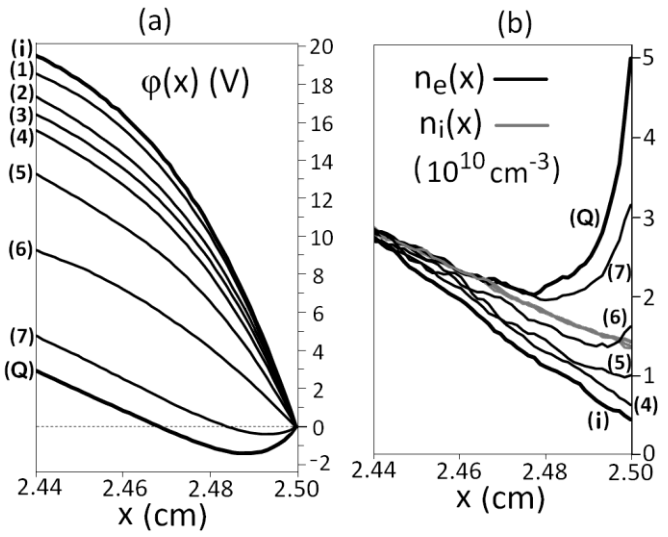

Fig. 5. Collapse of the sheath in time. (a) Potential profiles near the right wall, plotted relative to the wall for easy comparison. Initial state (i) at t = 497.5 ns represents the pre-collapse state with Φ = 38V, see Fig. 1(b). States (1) to (Q) are from t = 501.88 to 508 ns, corresponding to the temporal data points in Fig. 4. State (Q) is when quenching occurs. (b) Electron and ion density profiles during collapse. Labeled $n_e(x)$ profiles correspond to the $\varphi(x)$ profiles. States (1)-(3) for $n_e(x)$ are omitted due to strong overlap. $n_i(x)$ barely changes during collapse. The surface charge sign and magnitude can be inferred from $d\varphi(x)/dx$ at the wall by Gauss's law.

3. The Instability Quenches when the Surface Charge on the Wall Becomes Positive

It may be expected that the sheaths should fully collapse (Φ should reach 0), since there is no apparent way for the runaway drop of Φ to stop. But surprisingly, this does not occur. At t_2 = 508ns in Fig. 4, $\Gamma_{WC,R}$ reaches a maximum and simultaneously the decharging stops ($d\sigma_R/dt \approx 0$). The collapse has quenched but Φ only dropped to a minimum Φ_{min} = 18V (Fig. 2). In fact, Φ never approaches zero or becomes negative during any instability events in Fig. 2 and Fig. 3.

The reason for the quenching is that the runaway loss of electrons from the wall eventually leads to a surface charge that is positive ($\sigma > 0$, or $\sigma_e < 0$). When $\sigma > 0$, some emitted secondaries get pulled back to the wall, producing a new influx component Γ_{ref}. As the sheath collapses, σ will at some time become sufficiently positive to pull back the right fraction of secondaries to make the net electron flux $\Gamma_{e,net}$ equal Γ_{ion} again so that $d\sigma_e/dt \approx 0$ and $\gamma_{net} < 1$. The sheath is now I-V stable because there is a stabilizing collection term in (4) due to the fact that $d\Gamma_{ref}/d\Phi < 0$ when $\sigma_e < 0$.

The change in $\varphi(x)$ during sheath collapse is depicted in Fig. 5(a). The sheath amplitude is abruptly reduced over 7ns. As σ_e drops below 0, the SEE-suppressing field forms near the wall and $\varphi(x)$ becomes nonmonotonic. The potential "dip" amplitude when quenching occurs is 1.4V. This value

is of the order of the initial kinetic energies of true secondaries, which are emitted with an energy distribution corresponding to T_{emit} = 2eV.

The secondaries pulled back to the wall are colder than the hot WCE's and do not induce strong SEE. But due to how the simulation diagnostics work, they are also counted as WCE's in the data. This way the quenching of instability is apparent before t_2 in Fig. 4 as the effective γ_{WC} quickly drops from a peak value of 1.3 to a value slightly below unity. Hot "true" WCE's with $\gamma_{WC} \approx 1.3$ are still hitting the right wall because $\Phi_R < \Phi_{eq}$, but due to the contribution of Γ_{ref}, $\gamma_{WC,eff}$ saturates near 1.

The electrons removed from the wall during collapse become new secondaries which add to the negative space charge near the interface. Because of this, we find $n_e(x) > n_i(x)$ in the sheath at the quench state (Q) in Fig. 5(b). This is opposite to the usual structure of a Debye sheath like the pre-collapse state (i) where $n_i(x) > n_e(x)$.

To answer an earlier question, the reason the sheath does not fully collapse is that there is still a repulsive barrier to interior plasma electrons in state (Q) provided by the negative space charge from the new secondaries. This barrier is important because if Φ did drop to zero, all bulk electrons would be able to escape, causing a destructively high thermal power flux. Instead, the rate at which Φ decreases with σ_e (the coefficient α used in (16),(17)) is determined by the average spatial displacement of the lost surface electrons from the surface, which is limited by the slow emission velocities of secondaries (T_{emit}). We verified if T_{emit} is increased, Φ drops further during each instability. For sufficiently high T_{emit}, Φ can actually drop below zero.

The change in the field $E_x(x) = -d\varphi(x)/dx$ during collapse is localized near the wall in Fig. 5(a). Further away from the wall, the new secondaries have been accelerated to higher velocity, thereby minimizing the density change $\Delta n_e(x)$. We see near x = 2.44cm, $E_x(x)$ is almost unaffected throughout the collapse. Incidentally in Fig. 5(b), $n_i(x)$ does not change much during collapse due to the large ion mass and the fast time scale of the instability. As in RF discharges[2], the ion profiles $n_i(x)$, $\langle v_i \rangle(x)$ can be assumed static and Γ_{ion} constant as the sheath changes.

Interestingly, at the quench state (Q), φ(x) looks qualitatively similar to the SCL sheath[1,2,3,4,5,6,20] often expected to form at surfaces with very strong SEE. The sheaths were observed to transition briefly to a SCL-like state in past studies of instabilities[7,8], but it was not known why this happened. A SCL sheath theoretically arises when solving Poisson's equation with the plasma electron density, plasma ion density and secondary electron density written in terms of φ(x). When the SEE yield of hot plasma electrons crosses a critical threshold γ_{cr} near unity, the space charge due to the emission $\Gamma_{e,out} = \gamma_{net}\Gamma_{ion}/(1-\gamma_{net})$ becomes large enough to force a nonmonotonic φ(x) solution with a dip near the wall. A similar φ(x) with a dip or "virtual cathode" near the wall also appears for walls emitting strong thermionic electron current. Pointed out as early as Langmuir's work[33], a nonmonotonic or "double" sheath must arise in steady state to suppress some emission if the surface emits more than the plasma electron saturation current.

However, the nonmonotonic φ(x) in Fig. 5(a) is fundamentally different from a "real" steady state double sheath of any kind. For a valid *static* solution to Poisson's equation, $n_i(x)$ is expressible in terms of φ(x) by the familiar energy and flux conservation relations. But if the unperturbed state (i) is a static solution, the quench state (Q) clearly cannot be because φ(x) changed for all x while $n_i(x)$ is unchanged. The nonmonotonic φ(x) arising during sheath collapse is strictly a time-dependent effect caused by the sudden expulsion of surface electrons making $\sigma > 0$.

4. All WCE's escape the system

After the right wall sheath collapse has quenched at t_2 in Fig. 4, a brief period of current balance exists. At t_3, $\Gamma_{WC,R}$ remains very large because the sheath potential Φ_R is still at a smaller value Φ_{min} = 18V compared to Φ_{eq} = 38V. A similar sheath collapse occurred at the left wall at t ≈ 512ns and has quenched by $t = t_3$. So all electrons in the system with $e\Phi_{min} < w_x < e\Phi_{eq}$ will escape. The WCE's that escape are replaced by secondary electrons with w_x ranging from $e\Phi_{min}$ to $e\Phi_{eq}$.

The intense outflux of secondaries will cross the plasma and strike the other wall. This explains the large increase of Γ_b at each wall. $\Gamma_{b,L}$ and $\Gamma_{b,R}$ reach their peaks respectively at t_4 and t_5, about 13ns after sheath collapse quenches at the *other* wall. This implies that τ_{flight} for beam electrons is about 13ns. τ_{flight} is also the approximate time that it takes the detrapped WCE's with $e\Phi_{min} < w_x < e\Phi_{eq}$ to fully escape after collapse. Therefore the WCE's "run out" at around the same time Γ_b reaches its peak value at each wall. So by t_4 and t_5, $\Gamma_{WC,L}$ and $\Gamma_{WC,R}$ have respectively dropped to values much smaller than their peak values. Overall, the escape of the WCE's causes more than 10% of the plasma energy to be lost to the walls within a short (~20ns) time.

5. Restoration of the system to a new steady state

After a WCE instability, the system tends to restore to a new quasisteady state (Figs. 2 and 3). Note that the instability near t = 500ns in Fig. 2 causes a permanent dramatic change to all parameters. But all other instabilities in Fig. 2, and all instabilities in Fig. 3, transition all parameters (except γ_{WC}) roughly to the same pre-instability value. Something is mysteriously different about the first instability in Fig. 2.

To explain this anomaly, we continue where we left off from the previous section (t_5 in Fig. 4). For flux balance considerations: at t_5, Γ_b at each wall is far larger than it was before instability (~15 times) and Γ_{WC} is small again (relative to Γ_b). Γ_{CE} has increased due to the increase in size of the loss cone, but by less than a factor of two. γ_{CE} is weakly changed. To reach a new quasisteady state, Eq. (12) must be satisfied approximately, $\Gamma_b \approx \gamma_{CE}\Gamma_{CE}/(1-\gamma_b)$. There is a wide range of possible γ_b because with E_z = 200 V/cm and B_x = 100 G, the

energies of true secondaries impacting the walls could range anywhere from 0 to $2m_eV_D^2$ = 45eV via (14). Thus γ_b for BNC could vary in principle from zero to unity, depending on Φ. Since it is *always* the case after an instability that $\Gamma_b >> \Gamma_{CE}$, we see that Γ_b can remain much larger than its pre-instability value if the system restores to a Φ in which γ_b becomes closer to unity. This is what happens after the first instability of Fig. 2. However, when the second instability occurs, γ_b is already near 1, so all parameters tend to restore to their pre-instability value. Hence the instabilities following the first one become quasiperiodic.

To show more clearly how the new quasisteady state is reached after collapse, we illustrate a WCE instability occurring in another simulation with E_z = 100V/cm, $\nu_{turb} = 11.2\times10^6 s^{-1}$ and all else equal to the previous simulations. In Fig. 6, sheath collapse begins at the left wall first near t = 2843ns. The temporal behavior of the fluxes and partial SEE coefficients during instability are qualitatively similar to Fig. 4 up to when Γ_b reaches its peak value at each wall. The entire analysis of the collapse from the previous sections applies. $\Gamma_b >> \Gamma_{CE}$ at each wall after collapse as always. But there is a major difference when the system restores to a new quasisteady state. There is a large recharging of each wall ($d\sigma_e/dt > 0$) accompanied by a simultaneous decrease of Γ_b. Notice that Γ_b decreases all the way to a tenth of its peak value before a new quasisteady state was achieved near t = 2890 ns. In contrast, after the first instability in Fig. 4, there is minimal recharging and Γ_b remains near its peak value.

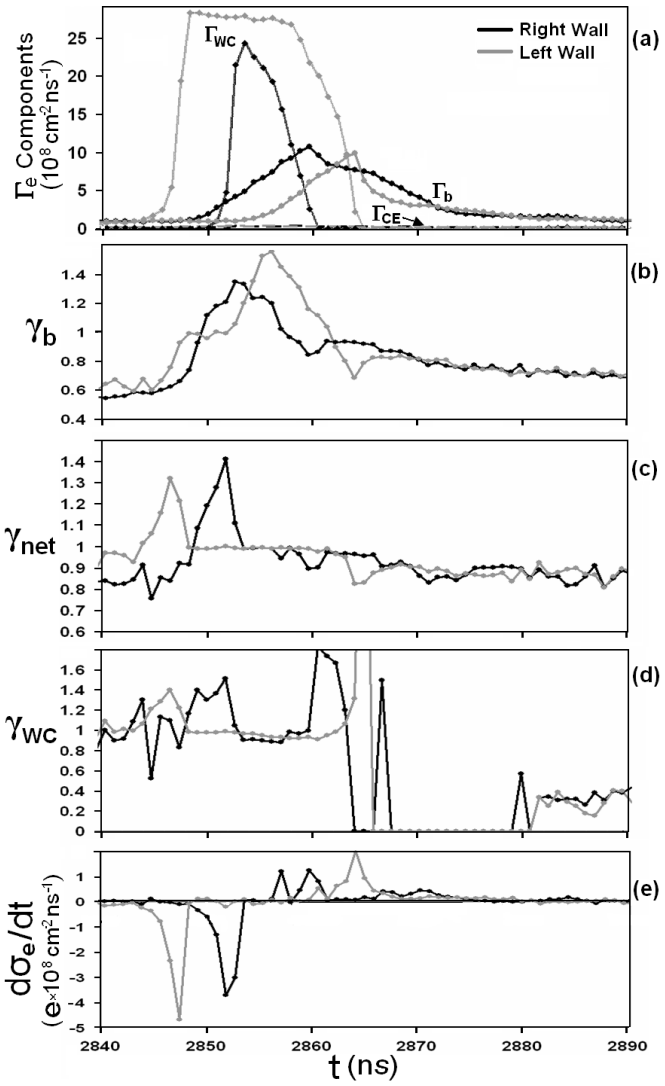

FIG. 6. Evolution of parameters during the first instability in a simulation with E_z = 100V/cm, $\nu_{turb} = 11.2\times10^6 s^{-1}$.

The reason for the difference is that with E_z = 100V/cm, the maximal drift energy true secondaries can gain is 11eV, only ¼ of that in the E_z = 200V/cm simulation. This puts an upper limit, well below 1, on the maximum possible steady state γ_b. Recall that the large increase of Γ_b after sheath collapse is produced by secondaries emitted from the other wall with a range of w_x; $e\Phi_{min} < w_x < e\Phi_{eq}$. So as the intense beam restores electrons to the wall, Φ increases above Φ_{min} and some incoming beam electrons get cut off by the larger potential barrier. This causes Γ_b to drop as the walls recharge in Fig 6. (The same decrease of Γ_b and increase of Φ also happen after the periodic instabilities of Fig. 2). The recharging makes $\sigma_e > 0$ again, thereby making $\varphi(x)$ monotonic. In all cases, recharging stops when a new quasisteady state is reached satisfying (12). γ_b was approximately 0.6 before instability in both Fig. 4 and Fig. 6. For the latter run with E_z = 100 V/cm, γ_b could only relax to

0.72 with $\Gamma_b \approx 6\Gamma_{CE}$ but in the E_z = 200 V/cm run γ_b was able to remain at 0.95 with $\Gamma_b \approx 19\Gamma_{CE}$.

In the E_z = 50V/cm simulation (Fig. 3) there are no significant changes in γ_b after any of the instability events, including the first one near t = 1.5 μs. Because $2m_eV_D^2$ is only 4eV in this run, ε_{beam} will not vary enough to change γ_b even as Φ varies widely (35V to 17V) throughout the first 6μs. One can confirm from (12) that the *gradual* increase of Γ_b over the first 3μs is driven by gradual increases of Γ_{CE} and γ_{CE}. Since γ_b is roughly fixed, there are no permanent jumps of Γ_b that we observed in the other two simulations, only temporary jumps during instabilities. In this run, γ_b is 0.55, larger than one would expect from impacting electrons with $\varepsilon \leq$ 4eV. This is due to the beam's elastically backscattered secondaries with high energies. Backscattering is also responsible for the large *temporary* increases of γ_b during instability. When a sheath collapses, there is a sudden jump of secondary flux $\Delta\Gamma_{e,out} \approx \gamma_{WC}\Delta\Gamma_{WC}$ from that wall. Some of these new secondaries are the high energy type, which travel at high velocity and strike the other wall with $\gamma(\varepsilon)$ well above 1. So γ_b can reach much higher values during instability (1.4 in Fig. 6) than during steady state because the backscattered fraction is temporarily larger. Once the colder true secondaries catch up, which is when Γ_b reaches its peak value, γ_b is much lower than its peak value.

6. Why is $\gamma_{WC} < 1$ after instability?

After the periodic instabilities of Fig. 2 and in Fig. 3, γ_{WC} is well below unity (~0.7 in Fig. 2 and ~0.4 in Fig. 3). As was observed in Fig. 4 of Ref. 8, the "WCE region" of the EVDF $e\Phi_{min} < w_x < e\Phi_{eq}$ now consists of trapped "former beam electrons" (FBE's). FBE's have smaller parallel energies than the hot bulk WCE's had *before* instability, so this is why $\gamma_{WC} < 1$ and the sheath is stable again. (The reader may wonder why γ_{WC} after restoration is not equal to γ_b. This is because the beam flux is produced by *coherent* true secondaries and backscattered electrons, while the FBE's are true secondaries with *mixed* drift phases.)

F. Under what plasma conditions does the WCE instability occur?

The equilibrium bulk EEDF in the simulation model is approximately bi-Maxwellian with temperatures $T_{//}$ and T_x, where $T_{//} \propto (E_z/B_x)^2(\nu_{turb}/\nu_{en})$.[29] $T_{//}$ and T_x are unequal due to the anisotropic heating and low collisionality. In simulations where $T_{//}$ exceeds a critical value, a steady state with $\gamma_{WC} < 1$ cannot exist. Periodic instabilities called "relaxation sheath oscillations" (RSO's)[8] occur. As the plasma "attempts" to relax to a bi-Maxwellian form with large $T_{//}$, γ_{WC} reaches unity, causing an instability which cools the WCE region of the EVDF to make $\gamma_{WC} < 1$ temporarily. The period of "oscillation" seen in Fig. 2 and Fig. 3 is governed by the time it takes the WCE region to reheat after each instability. This time is unrelated to (and orders of magnitude larger than) the period of plasma oscillations. When RSO's occur, the zero current condition is only maintained in a time-averaged sense over the RSO period. This contrasts to time-independent sheath theories that require zero current at all times at a dielectric surface.

An estimate $T_{//,cr} \sim$ 40eV of the critical $T_{//}$ needed for the onset of RSO's was found by integrating $\gamma(\varepsilon)$ for BNC over a 2-D Maxwellian. For lower temperature simulations, an equilibrium is reached with $\gamma_{WC} < 1$. A finite number of instabilities may still occur as the system evolves from its irregular initial state at t = 0 to its equilibrium[7], which takes ~5-10μs due to the slow adjustment of ions. The $\varphi(x)$ snapshot in Fig. 1(b) taken early in the simulation has a rather flat region in the middle because the interior ions have not yet reacted to the sheath formation. $\varphi(x)$ in a true equilibrium looks (qualitatively) parabolic[28].

Interestingly, it was found in Ref. 7 that equilibrium states always have SEE beams that undergo (n+3/4) number of rotations before impact. The proposed explanation for this was that if Φ changes, τ_{flight} changes in Eq. (14), which changes γ_b, thereby changing the emitted flux, which changes σ_e. And therefore the "differential resistance" of the sheath was only stable if $d\gamma_b/d\Phi > 0$, requiring that the beam phase be within certain allowed bands (see Fig. 4 of Ref. 7). The theory relies on the two sheaths evolving simultaneously and the SEE beams always being the dominant flux. This is valid for *quasisteady* evolution over many μs (1μs >> τ_{flight}), because $\varphi(x)$ stays symmetric and Φ changes so slowly that Γ_{WC} remains small (as in the stable intervals of Fig. 2). So the theory accurately explains the stability bands. However, we have confirmed that the above differential resistance mechanism is not related to sheath collapse and is not the reason the beam phase can change abruptly after a sheath collapse; Fig. 4 and Fig. 6 show that (a) the sheaths collapse asymmetrically one at a time, (b) that they collapse faster than τ_{flight} and (c) that the WCE flux dominates.

We note that the WCE instability does not require the planar geometry, perfect symmetry, normal B-field, low collisionality or floating surfaces used in the simulations here. We have confirmed that similar instabilities do occur in variations of the simulation model that are asymmetric and/or use biased walls.

IV. IMPLICATIONS OF SHEATH INSTABILITIES ON TRANSPORT AND ENERGY LOSS

The study of electron transport in crossed electric and magnetic fields is an important fundamental plasma physics problem not just for E×B discharges[27,34] where the **E** field is externally applied. It is also important in cases where the **E** field is generated by the ambipolar constraint[35], from PSI (e.g. drifts within sheaths[36]) or from biased surfaces contacting the plasma (e.g. plasma perturbation and cross-field effects from probes[40,37,38] or biased divertor plates[39]).

Common cross-B-field transport mechanisms include viscosity, inertia and ion-neutral collisions[40] in the bulk plasma. But emitted secondaries from the *surface* can also cause transport. True secondaries, as well as impacting electrons that randomly backscatter, will on average suffer a displacement across **B** comparable to the gyro-radius in the direction of **E**. This near-wall conductivity (NWC) effect[41] is known to be very important in HT's and can outweigh transport from turbulence. Experimental evidence of NWC comes from the strong influence of the wall material on the discharge current[27,42,43,45]. For a given discharge voltage, the axial current is larger when emitting materials are used. As the voltage is increased, the SEE conductivity causes saturation of the plasma temperature and axial electric field in the channel[44].

Sheath instabilities could exacerbate the degrading SEE-induced transport. 2-D (r,θ) simulations of a HT by Taccogna *et. al*[10] showed that azimuthal field fluctuations driven by a radial sheath instability can strongly increase transport. While the azimuthal dimension is not included in the 1-D EDIPIC model, one could expect a similar result for a WCE sheath collapse if it were propagating along a cylindrical channel or any 1-D or 2-D surface.

Sheath instabilities can also excite waves in the bulk plasma. It is impossible to maintain exact neutrality in the plasma when the surface potential rapidly changes because the charge density contributed by electrons moving away from the surface also changes, generating net charge perturbations. Plasma thruster experiments in Ref. 17 and references therein found a connection between SEE, spontaneous microwave oscillations and anomalous wall erosion. The SEE-driven oscillations in Ref. 15 were found to launch ion acoustic waves.

One implication of WCE instabilities in particular for HT's is that they transition the system to a state that has the maximum γ_b and Γ_b allowed by current balance considerations (Sec. III.D.5). The detrimental effect the beams could have on HT performance is evident when comparing the 200V/cm run (Fig. 2) with the 50V/cm run (Fig. 3). Both runs were configured to have a similar bulk plasma temperature (by choosing a different ν_{turb}). For this reason, γ_{CE} and Γ_{CE} are similar in both runs. But because the 200V/cm run has SEE beams with γ_b close to 1 in (12), the total influx and axial transport is far larger.

The consequences of secondaries passing between surfaces are not captured in fluid models[45,46,47] of HT's. Secondaries reaching other surfaces have been observed in simulations by other authors with other PIC codes[48]. Experimental proof of this has not been published to our knowledge. But HT experiments have shown that the discharge current also increases up to saturation when decreasing the radial magnetic field at a fixed voltage[45]. This is consistent with the theory that SEE-driven transport could be related to the SEE yield of the beams γ_b, which is determined by the *ratio* E_z/B_x.

V. CONCLUSIONS

The Debye sheath is usually assumed to be a static structure. We presented a general theory showing various conditions under which sheaths can become unstable due to secondary electron emission. In particular, we showed that whenever a plasma's electron temperature exceeds a critical value, the I-V trace of a surface contacting the plasma always has a negative differential resistance branch which can drive instability phenomena. For a Maxwellian plasma EEDF, the critical value is simply the temperature in which the SEE coefficient exceeds unity for the surface material, a condition already known to be met in applications[23].

As a practical example, we studied by simulation the time evolution of a sheath instability predicted to occur under experimental conditions in Hall thrusters. The instability causes a runaway loss of electrons from the surface and corresponding collapse of the sheath amplitude. It was shown that the charge density distributions and wall fluxes found during instability were not physically possible steady states of a sheath structure. In other words, the dynamic sheaths are not equivalent to stable sheaths evolving quasistatically, and hence cannot be understood in terms of time-independent PSI theories. In addition, instabilities caused major changes in the potential profile, wall fluxes, energy loss, cross-B-field transport and the bulk plasma EVDF.

Simulations are useful for studying sheath instabilities since secondary electrons can be tracked and the sheath structure can be studied closely in time. But experiments do not have this advantage. In plasma devices, observed changes resulting from SEE-driven instabilities may be overlooked and assumed to be driven by processes in the plasma interior. In light of the nonsteady sheath effects observed in this paper and elsewhere in the literature[7,8,9,10,11,12,13,14,15,16,17], a static sheath cannot be taken for granted in practice when SEE is very strong.

ACKNOWLEDGMENTS

This work was supported by the U.S. Department of Energy and the U.S. Air Force Office of Scientific Research. D. Sydorenko was the primary developer of the EDIPIC simulation code used in this paper. The authors thank Y. Raitses for helpful discussions.

[1] G.D. Hobbs and J.A. Wesson, Plasma Phys. **9**, 85 (1967).
[2] M. A. Lieberman and A. J. Lichtenberg: *Principles of Plasma Discharges and Material Processing* (Wiley, Hoboken, NJ, 2005).
[3] L. A. Schwager, Phys. Fluids B **5**, 631 (1993).
[4] P. C. Stangeby, *The Plasma Boundary of Magnetic Fusion Devices*, Plasma Phys. Series (IOP, Bristol, 2000).
[5] E. Ahedo, Phys. Plasmas **9**, 4340 (2002).
[6] I.V. Tsvetkov and T. Tanabe, J. Nucl. Mat. **266**, 714 (1999).
[7] D. Sydorenko, A. Smolyakov, I. Kaganovich and Y. Raitses, Phys. Plasmas **15**, 053506 (2008).

[8] D. Sydorenko, I. Kaganovich, Y. Raitses and A. Smolyakov, Phys. Rev. Lett. **103**, 14 (2009).
[9] M.D. Campanell, A.V. Khrabrov and I.D. Kaganovich, Phys. Rev. Lett. **108**, 235001 (2012).
[10] F. Taccogna, S. Longo, M. Capitelli, and R. Schneider, Appl. Phys. Lett. **94**, 251502 (2009).
[11] F. Zhang, D. Yu, Y. Ding, and H. Li, Appl. Phys. Lett. **98**, 111501 (2011).
[12] F. Zhang, Y. Ding, H. Li, X. Wu and D. Yu, Phys. Plasmas **18**, 103512 (2011).
[13] F. Taccogna, S. Longo, M. Capitelli and R. Schneider, Nuovo Cimento B **125**, 529 (2010).
[14] A.I. Morozov and V.V. Savel'ev, Plasma Phys. Rep. **28**, 1017 (2002).
[15] M.C. Griskey and R.L. Stenzel, Phys. Rev. Lett. **82**, 556 (1999).
[16] K.P. Kirdyashev, Tech. Phys. Lett. **23**, 395 (1997).
[17] K. P. Kirdyashev and V.I. Brukhty, Proc. 3rd International Conference on Spacecraft Prop., Cannes, 2000, pp. 849-854.
[18] A. I. Morozov, Sov. J. Plasma Phys. **17**, 393 (1991).
[19] C. Nam, N. Hershkowitz, M. H. Cho, T. Intrator and D. Diebold, J. Appl. Phys. **63**, 5674 (1988).
[20] J. Seon, E. Lee, W. Choe and H. Lee, Curr. Appl. Phys. **12**, 663 (2012).
[21] M.D. Campanell, A.V. Khrabrov and I.D. Kaganovich, Phys. Rev. Lett. **108**, 255001 (2012).
[22] J.R.M. Vaughan, IEEE Trans. Electron Devices **36**, 1963 (1989).
[23] C.A. Ordonez and R.E. Peterkin Jr., J. Appl. Physics. **79**, 2270 (1996).
[24] E. Ahedo and F.I. Parra, Phys. Plasmas **12**, 073503 (2005).
[25] D. Sydorenko, Ph.D. thesis, U. of Saskatchewan, 2006.
[26] Y. Raitses, A. Smirnov, D. Staack and N.J. Fisch, Phys. Plasams. **13**, 014502 (2006).
[27] Y. Raitses, I.D. Kaganovich, A. Khrabrov, D. Sydorenko, N.J. Fisch, and A. Smolyakov, IEEE Trans. Plasma Sci. **39**, 995 (2011).
[28] D. Sydorenko, A. Smolyakov, I. Kaganovich and Y. Raitses, Phys. Plasmas **13**, 014501 (2006).
[29] I.D. Kaganovich, Y. Raitses, D. Sydorenko and A. Smolyakov, Phys. Plasmas **14**, 057104 (2007).
[30] A.B. Langdon, B.I. Cohen and A. Friedman, J. Comput. Phys. **51**, 107 (1983).
[31] A. Smirnov, Y. Raitses, and N. Fisch, Phys. Plasmas **11**, 4922 (2004).
[32] A. Dunaevsky, Y. Raitses and N.J. Fisch, Phys. Plasmas **10**, 2574 (2003).
[33] I. Langmuir, Phys. Rev. **33**, 954 (1929).
[34] M. Keidar and I. Beilis, IEEE Trans. Plasma Sci. **34**, 804 (2006).
[35] J.D. Callen, A.J. Cole and C.C. Hegna, Phys. Plasmas **16**, 082504 (2009).
[36] R.H. Cohen and D.D. Ryutov, Phys. Plasmas **2**, 2011 (1995).
[37] A. Carlson, Phys. Plasmas **8**, 4732 (2001).
[38] D. Staack, Y. Raitses and N. J. Fisch, Rev. Sci. Inst. 75, 393 (2004).
[39] R.H. Cohen, D.D. Ryutov, G.F. Counsell and P. Helander, Plasma Phys. Control. Fusion **49**, 1 (2007).
[40] V.A. Rozhansky, A.A. Ushakov, and S.P. Voskboynikov, Nucl. Fusion, **39**, 613 (1999).
[41] A.I. Morozov, Sov. J. Plasma Phys. **3**, 19 (1968).
[42] Y. Raitses, M. Keidar, D. Staack, and N.J. Fisch, J. Appl. Phys. **92**, 4906 (2002).
[43] N. Gascon, M. Dudeck and S. Barral, Phys. Plasmas **10**, 4123 (2003).
[44] Y. Raitses, D. Staack, A. Smirnov and N.J. Fisch, Phys. Plasmas **12**, 073507 (2005).
[45] S. Barral, K. Makowski, Z. Peradzynski, N. Gascon, and M. Dudeck, Phys. Plasmas **10**, 4137 (2003).
[46] E. Ahedo, J.M. Gallardo and M. Martinez-Sanchez, Phys. Plasmas. **10**, 3397 (2003).
[47] M. Keidar, I.D. Boyd and I.I. Beilis, Phys. Plasmas **8**, 5315 (2001).
[48] F. Taccogna, S. Longo, M. Capitelli and R. Schneider, Contrib. Plasma Phys. **48**, 375 (2008).

The Princeton Plasma Physics Laboratory is operated
by Princeton University under contract
with the U.S. Department of Energy.

Information Services
Princeton Plasma Physics Laboratory
P.O. Box 451
Princeton, NJ 08543

Phone: 609-243-2245
Fax: 609-243-2751
e-mail: pppl_info@pppl.gov
Internet Address: http://www.pppl.gov